

Magnetic anisotropy and stability of Fe_3Ga compounds

T.M. Inerbaev¹, A.U. Abuova¹, A.K. Dauletbekova¹,
F.U. Abuova^{*,1}, G.A. Kaptagay², Zh. Zakieva¹,
M. Eltizarova¹, A. Barakov¹

¹L.N. Gumilyov Eurasian National University, Nur-Sultan, Kazakhstan

²Kazakh national women's teacher training University, Almaty, Kazakhstan

E-mail: fatika_82@mail.ru

DOI: 10.32523/ejpfm.2021050407

Received: 25.11.2021 - after revision

The magnetic anisotropy energy and the stability of crystal modifications of $D0_3$ and $L2_1$ of Fe_3Ga compounds are studied with the density functional theory methods. The magnetic anisotropy energy of the $D0_3$ structure is more than twice the same value for the $L2_1$ structure. The features in the electronic structure lead to the difference in the magnitude of spin-orbit interaction, explaining the found effect. The $L2_1$ structure is more thermodynamically stable in the entire range of the considered pressures. Under pressure, the considered crystal modifications of Fe_3Ga lose their stability due to the appearance of imaginary frequencies in their phonon spectra.

Keywords: Magnetic anisotropy, Band structure, Magnetostriction, Correlations, Phase mixture.

Introduction

Materials with high magnetostriction are widely used as magnetic field sensors, magneto-mechanical drives, and energy collectors [1]. A large, and sometimes preferably linear, response of the magnetic field is essential [2]. Giant magnetostriction up to 2000 ppm is contained in rare-earth alloys based on iron Terphenol and Terphenol-D [3, 4]. However, the cost of these materials is high due to the use of a large number of rare-earth elements. In addition, their hardness and brittleness are very high, limiting the scope of applying materials. $\text{Fe}_{1-x}\text{Ga}_x$ binary alloys (Galfenol) combine numerous advantages, such as a

sufficiently large magnetostriction coefficient, a low magnetic saturation field, excellent plasticity, and low cost [5-7]. Experimental studies of $\text{Fe}_{1-x}\text{Ga}_x$ have shown that the tetragonal magnetostriction coefficient λ_{001} in the concentration range $0 < x < 0.35$ shows a two-peak behavior near $x = 0.19$ and $x = 0.27$. The value of the magnetostriction coefficient for Galfenol reaches 400 ppm [8-10].

In a small concentration of Ga, the alloy has the structure A2 – an disordered solid solution of Ga atoms in a bcc-Fe lattice. The single-phase A2 demonstrates a monotonic growth of λ_{001} with the addition of Ga. The phase mixture (A2 + D0₃) leads to a rapid drop of λ_{001} after the first maximum, and alloys with 22.5-28 at.% Ga are single-phase. The D0₃ phase, which also shows a monotonic growth with the addition of Ga [11]. A further decrease in λ_{001} is associated with the formation of a mixture of phases (D0₃ + B2). The cooling rate changes amount of metastable inclusions in the alloy controlling the magnitude of magnetostriction within certain limits. [11-14] When heated, an irreversible phase transition of the first kind occurs in the $\text{Fe}_{1-x}\text{Ga}_x$ alloy from the metastable phase D0₃ to the equilibrium phase L1₂ [12, 13, 15] Fe with the structure A2, B2 and D0₃. $\text{Fe}_{1-x}\text{Ga}_x$ alloys have positive magnetostriction, and an alloy with the structure L1₂ has negative magnetostriction [15-18].

In addition to the long-range order and phase mixing, the short-range order also affects the material's properties. It has been shown that the "B2-like" structure with Ga-Ga atom pairs are formed along the $\langle 100 \rangle$ direction. These pairs are responsible for the observed magnification of magnetostriction in the $\text{Fe}_{1-x}\text{Ga}_x$ alloy with the A2 structure [19]. Analysis by differential X-ray absorption spectroscopy confirmed the existence of such pairs. The macroscopically observed magnetostriction occurs from the Ga medium. The Ga-Ga pairs themselves do not contribute to the intensification of magnetostriction. Magnetostrictive deformation near the Ga-Ga pairs, but not the defects themselves, are the source of magnification of magnetostriction [20].

Correlations of type B2 grow for quenched samples with high concentrations of Ga. Between 13 and 20.3 at.%, D0₃-type nanoclusters are observed, the size of which increases with increasing Ga concentration for both slowly cooled and quenched samples [21]. The D0₃ crystal structure or modified D0₃ nano-inclusions (L6₀ structure) in the A2 matrix are strongly distorted regarding cubic symmetry, having a localized symmetry of tetragonal or lower. [22, 23] sharp suppression of magnetostriction about 20 at.% Ga may be associated with a rapid increase in the near-order immediately before beginning the long-range chemical order. [21] This conclusion is confirmed by computer modeling [24]. Theoretical studies show B2-like D0₃ nanostructures cause magnetostriction with opposite signs indicating the short-range ordering is not of primary importance in increasing magnetostriction [25, 26].

In this paper, we carry out a theoretical comparison of the elastic properties and magnetic anisotropy energies (MAE) of Fe₃Ga polymorphs. D0₃ and L2₁ types of lattices are observed experimentally as macroscopic phases. Elastic properties and MAE are the key parameters that determine the magnetostrictive properties of materials [19].

Research methods

The first-principle calculations of the structural and magnetic properties of Fe-Ga alloy systems were performed using VASP (Vienna Ab-initio Simulation Package) [27, 28]. The exchange-correlation potential was considered using the generalized gradient approximation (GGA) in the form of Perdew-Burke-Ernzerhof (PBE) [29]. The grid of k-points was constructed on the basis of a grid centered at the G-point with a partition of $6 \times 6 \times 6$ points for the $D0_3$ structure, and $8 \times 8 \times 8$ for the $L1_2$ lattice. Pseudopotentials PAW [20, 21] with the configuration of valence electrons Fe ($3s^2 3p^6 3d^7 4s^1$), Ga ($3d^{10} s^2 4p^1$) were used to describe electron-ion interactions. Data preparation for calculations and subsequent processing was carried out using the VASPKIT package [30].

The model cells of the studied structures are shown in Figure 1. The unit cell of the lattice $D0_3$ ($Fm\bar{3}m$ group, #225) contains 16 atoms, while the lattice $L2_1$ ($Pm\bar{3}m$ group, #221) contains 4 atoms. There are two types of Fe atoms in the $D0_3$ structure, depending on their local environment. Namely, atoms of the Fe1 type, in the immediate environment of which there are other Fe atoms, and atoms of the Fe2 type, surrounded by 4 Fe1 atoms and 4 Ga atoms.

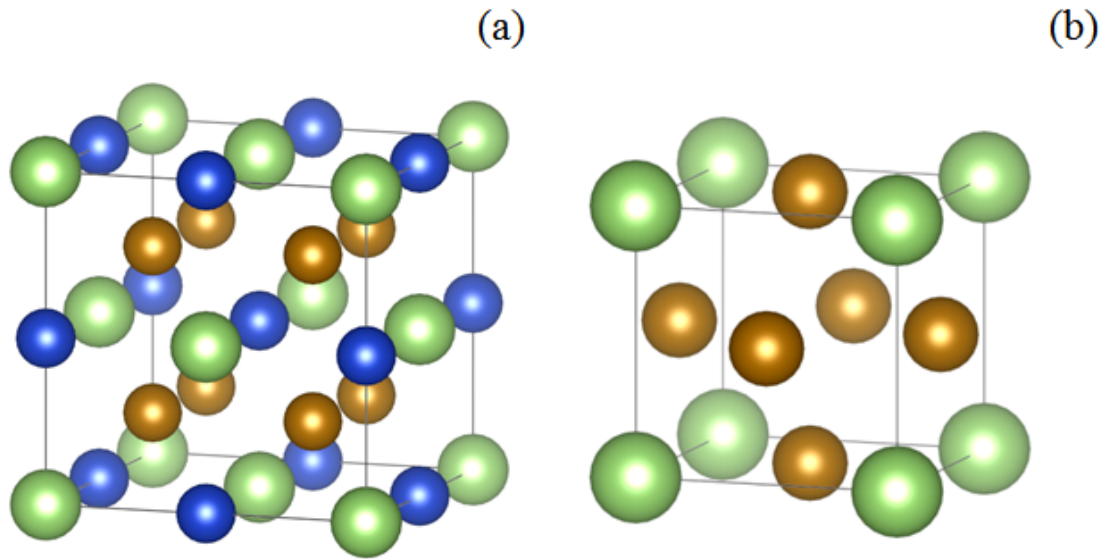


Figure 1. Model cells of structures (a) $D0_3$ and (b) $L2_1$. Ga atoms are shown as green spheres, Fe atoms are yellow. For the $D0_3$ structure, atoms of the Fe1 and Fe2 types are shown in blue and yellow colors, respectively.

Results and discussion

The calculated values of the magnetic anisotropy energy E_{MCA} are presented in Table I. E_{MCA} is the maximum value of the energy difference of the magnetic system when the spins are directed along the quantization axis $\langle 001 \rangle$, and when the spins are directed along some other direction. In the cases considered in this paper, these directions correspond to the vector $\langle 111 \rangle$ and are symmetrically equivalent. It can be seen that the E_{MCA} for the $D0_3$ structure is more than two times greater than the corresponding value for the $L1_2$ structure.

To explain this effect, it should be remembered that E_{MCA} is actually determined by the value of the spin-orbit coupling (SOC) energy, which can be written as [31] in the framework of perturbation theory

$$E^{SOC} = -\zeta^2 \sum_{o,u} \frac{|\langle o | \hat{\sigma} \cdot \hat{L} | u \rangle|^2}{\epsilon_u - \epsilon_o} \quad (1)$$

where $|o\rangle$ and $|u\rangle$ is the wave function of the occupied and unoccupied orbitals, ϵ_u and ϵ_o – energy of the corresponding orbitals, $\hat{\sigma}$ and \hat{L} – Pauli matrix and the operator of angular momentum, respectively.

Thus, the E^{SOC} value is determined by the difference $\epsilon_u - \epsilon_o$ in the denominator and the value of the matrix element in the numerator of Equation 1. The following matrix elements give a non-zero contribution from the d-states to the E^{SOC} :

$$\begin{aligned} \langle d_{xy} | \hat{L}_z | d_{yz} \rangle &= 1, \quad \langle d_{x^2-y^2} | \hat{L}_z | d_{xz} \rangle = 2, \quad \langle d_{z^2} | \hat{L}_x | d_{yz} \rangle = \sqrt{3}, \\ \langle d_{xy} | \hat{L}_x | d_{xz,yz} \rangle &= 1, \quad \langle d_{xy} | \hat{L}_x | d_{xz,yz} \rangle = 1, \quad \langle d_{x^2-y^2} | \hat{L}_z | d_{xz,yz} \rangle = 1 \end{aligned} \quad (2)$$

To analyze how the contributions of various states are formed in the E^{SOC} , an analysis of the band structure of compounds $D0_3$ and $L1_2$ was carried out. The results are shown in Figure 2. The most interesting areas of the band structure are where the distance between the free and occupied levels is minimal. In the $D0_3$ structure, this corresponds to the states near point X of the Brillouin zone. The matrix elements between the states d_{xy} (spin-down) and d_{z^2} (spin-up) will give the most significant contribution to E^{SOC} . The difference $\epsilon_u - \epsilon_o$ is approximately 0.1 eV. In the case of the $L1_2$ structure, the distance between the energy levels near point X is also the smallest for this compound. However, on the one hand, the value of $\epsilon_u - \epsilon_o$ is greater here than for the $D0_3$ structure, and, in addition, the corresponding energy levels are formed by the states d_{z^2} and $d_{x^2-y^2}$, which do not give non-zero matrix elements in Equation 2. Thus, E^{SOC} is formed by states for which the difference $\epsilon_u - \epsilon_o$ is much greater than the corresponding value for the $D0_3$ structure, which explains the effect of a smaller E^{MCA} value for the $L1_2$ compound compared to $D0_3$.

We also analyzed the stability of compounds $D0_3$ and $L1_2$. For this purpose, their enthalpies were calculated, that shown in Figure 3. It can be seen that the $L1_2$ structure is more energetically advantageous in the considered pressure range from 0 to 3 GPa. With a further increase in pressure, the compounds lose their dynamic stability, i.e., imaginary frequencies appear in the phonon spectra, as shown in Figure 4. Thus, these crystals can exist only at relatively low pressures.

Table 1.

The E_{MCA} energies of Fe_3Ga compounds of the $D0_3$ and $L1_2$ structures.

Structure	$E_{MCA}, \mu \text{ eV/f.u.}$
$D0_3$	17.9
$L1_2$	8.3

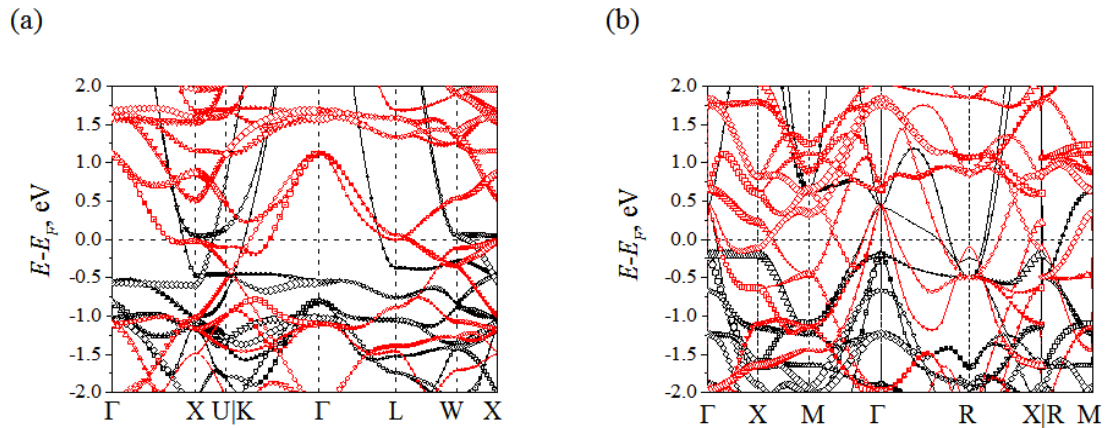


Figure 2. Calculated band structures for Fe_3Ga compounds (a) D0_3 and (b) L1_2 . The symbols mean the formation of the corresponding zones by electrons with wave functions: \square - d_{xy} , \circ - d_{yz} , \triangle - d_{xz} , ∇ - d_{z^2} , \diamond - $d_{x^2-y^2}$. The size of the symbols is proportional to the population of the level. Black lines and symbols indicate electronic states with a spin-up, red-with a spin-down.

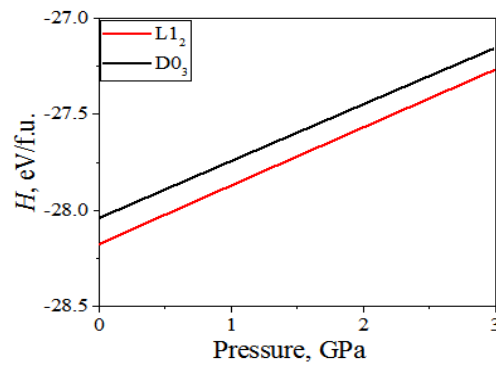


Figure 3. Enthalpy of phases D0_3 and L1_2 .

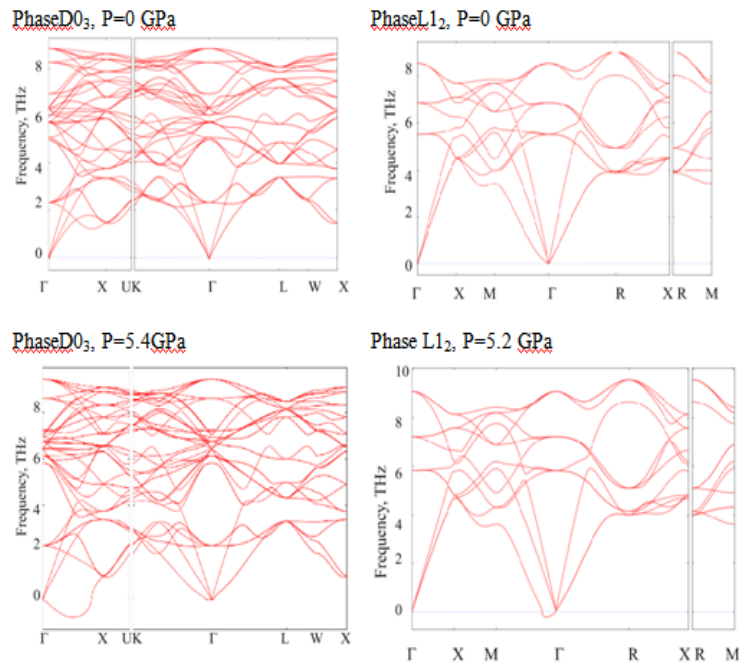


Figure 4. Phonon spectra of phases D0_3 and L1_2 at different pressures.

Conclusion

Fe_3Ga compounds of the D0_3 and L1_2 structures were studied. It is found that the magnetic anisotropy energy of the D0_3 structure is more than twice the

same value for the $L1_2$ structure. The band structure analysis showed that this effect is explained by the features of the electronic structure of the compound of the crystal modification $D0_3$ near point X of the Brillouin zone. Near this point, the occupied and free electronic states are located near the Fermi level. They are formed by d-states such that they give a non-zero contribution to the matrix elements that determine the magnitude of the spin-orbit interaction. In the $L1_2$ structure, the contribution to the spin-orbit interaction is determined by the electron levels located far from each other. Modeling the thermodynamic properties of the studied phases showed that the $L1_2$ structure is more stable over the entire range of the considered pressures. The considered crystal modifications of Fe_3Ga lose their stability due to the appearance of imaginary frequencies in their phonon spectra.

Acknowledgments

This work was carried out within the framework of the grant project AP08855879 "First principles design of effective magnetostriction materials for practical applications" for 2020-2022 of the Ministry of Education and Science of the Republic of Kazakhstan.

References

- [1] G. Engdahl, Handbook of giant magnetostrictive materials: A volume in Electromagnetism (Academic, San Diego, 2000). [[CrossRef](#)]
- [2] E. du Tremolet de Lacheisserie et al., Magnetism (Springer-Verlag, New York, 2005) 517 p. [[CrossRef](#)]
- [3] F. Jerems et al., Ferroelectrics **228**(1) (1999) 333-341. [[CrossRef](#)]
- [4] J.D. Verhoeven et al., Journal of Applied Physics **66**(2) (1989) 772-779. [[CrossRef](#)]
- [5] J. Atulasimha, A.B. Flatau, Smart Materials and Structures **20**(4) (2011) 043001. [[CrossRef](#)]
- [6] A.E. Clark et al., Journal of Applied Physics **93**(10) (2003) 8621-8623. [[CrossRef](#)]
- [7] A.E. Clark et al., IEEE Transactions on Magnetics **36**(5) (2000) 3238-3240. [[CrossRef](#)]
- [8] E.M. Summers et al., Journal of Materials Science **42**(23) (2007) 9582-9594. [[CrossRef](#)]
- [9] Q. Xing et al., Acta Materialia **56**(16) (2008) 4536-4546. [[CrossRef](#)]
- [10] A. Clark et al., Journal of Applied Physics **97** (2005) 10M316. [[CrossRef](#)]
- [11] Q. Xing et al., Acta Materialia **56**(16) (2008) 4536-4546. [[CrossRef](#)]
- [12] I. Golovin et al., Intermetallics **114** (2019) 106610. [[CrossRef](#)]
- [13] M.V. Matyunina et al., Phase Transitions **92**(2) (2019) 101-116. [[CrossRef](#)]
- [14] A.A. Emdadi et al., Journal of Alloys and Compounds **619** (2015) 58-65. [[CrossRef](#)]
- [15] I. Golovin et al., Journal of Alloys and Compounds **751** (2018) 364-369. [[CrossRef](#)]

- [16] N. Srisukhumbowornchai, S. Guruswamy, Journal of Applied Physics **92**(9) (2002) 5371-5379. [[CrossRef](#)]
- [17] T.V. Jayaraman et al., Journal of Applied Physics **102**(5) (2007) 053905. [[CrossRef](#)]
- [18] I.S. Golovin et al., Journal of Alloys and Compounds **811** (2019) 152030. [[CrossRef](#)]
- [19] R. Wu, Journal of Applied Physics **91** (2002) 7358-7360. [[CrossRef](#)]
- [20] M.P. Ruffoni et al., Phys. Rev. Lett. **101** (2008) 147202. [[CrossRef](#)]
- [21] Y. Du et al., Physical Review B **81**(5) (2010) 054432. [[CrossRef](#)]
- [22] H. Cao et al., Phys. Rev. Lett. **102** (2009) 127201. [[CrossRef](#)]
- [23] T. Lograsso et al., Journal of Alloys and Compounds **350**(1-2) (2003) 95-101. [[CrossRef](#)]
- [24] H. Wang et al., Scientific Reports **3**(1) (2013) 3521. [[CrossRef](#)]
- [25] H. Wang et al., Applied Physics Letters **97**(26) (2010) 262505. [[CrossRef](#)]
- [26] M. Huang et al., Applied Physics Letters **95**(17) (2009) 171907. [[CrossRef](#)]
- [27] G. Kresse, D. Joubert, Phys. Rev. B **59** (1999) 1758-1775. [[CrossRef](#)]
- [28] G. Kresse, J. Furthmuller, Phys. Rev. B **54** (1996) 11169-11186. [[CrossRef](#)]
- [29] J.P. Perdew et al., Phys. Rev. Lett. **78** (1997) 1396-1396. [[CrossRef](#)]
- [30] V. Wang et al., Computer Physics Communications **267** (2021) 108033. [[CrossRef](#)]
- [31] D.-Sh. Wang et al., Phys. Rev. B **47** (1993) 14932-14947. [[CrossRef](#)]